

Learning a Compact State Representation for Navigation Tasks by Autoencoding 2D-Lidar Scans

Christopher Gebauer

Maren Bennewitz

Abstract—In this paper, we address the problem of generating a compact representation of 2D-lidar scans for reinforcement learning in navigation tasks. By now only little work focuses on the compactness of the provided state, which is a necessary condition to successfully and efficiently train a navigation agent. Our approach works in three stages. First, we propose a novel preprocessing of the distance measurements and compute a local, egocentric, binary grid map based on the current range measurements. We then autoencode the local map using a variational autoencoder, where the latent space serves as state representation. An important key for a compact and, at the same time, meaningful representation is the degree of disentanglement, which describes the correlation between each latent dimension. Therefore, we finally apply state-of-the-art disentangling methods to improve the representation power. Furthermore, we investigate the possibilities of incorporating time-dependent information into the latent space. In particular, we incorporate the relation of consecutive scans, especially egomotion, by applying a memory model. We implemented our approach in python using tensorflow. Our datasets are simulated with pybullet as well as recorded using a slamtec rplidar A3. The experiments show the capability of our approach to highly compress lidar data, maintain a meaningful distribution of the latent space, and even incorporate time-dependent information.

I. INTRODUCTION

In recent years a variety of mobile robots became available at the consumer market for a reasonable price and keep improving their astonishing capabilities. One of the most fundamental tasks for an operating robot is to safely navigate within the environment. Most systems today are capable of considering the nearby surroundings based on sensor data, and even react reasonable to moving obstacles if their motion is mathematically describable. In more complex situations, e.g., when close interactions with humans are involved, classical approaches are still able to successfully navigate [1]. However, to further improve the rather short-sighted and reactive behavior deep reinforcement learning (RL) has been applied, to achieve a navigation policy, that results in a more socially compliant robot behavior [2].

To be able to learn a navigation policy, a precise observation of the surroundings is required. For indoor tasks a common choice is a 2D-lidar sensor, as it is robust and cheap. The drawbacks are the high dimensionality of the data and the hidden information due to its representation, as the angle θ of each range measurement is only recoverable with additional knowledge. In a RL setup the usage of raw sensor

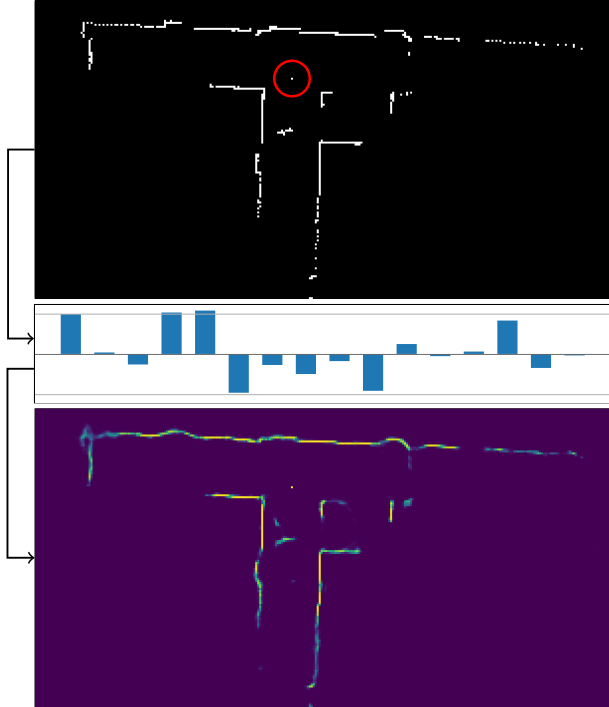


Fig. 1: The representation of the 2D-lidar scan at three different stages of our autoencoding pipeline. The top view shows a local image, which is passed as input. The robot pose is highlighted with a red circle. The bar plot in the middle shows the compressed state representation, which we lay our interest on in this work. Based on this compact state, the entire image at the bottom is reconstructed. It represents the distribution over the original image, where brighter regions show a higher probability of a pixel being occupied. Even though not directly visible for humans, a correlation between specific dimensions of the latent space and outer factors, e.g., wall orientation exists.

measurements usually causes the agent to learn sluggishly and perform poorly in certain situations. This effect has been shown on the example of RGB images by Yarats *et al.* [3]. To overcome this, a powerful representation is either trained in advance [4], or concurrently but with stronger auxiliary losses [5]. Commonly, both approaches are based on an autoencoder (AE) architecture. The general idea of an AE is to compress an input into a latent space, where the target is to losslessly reconstruct the input based on this latent space. Even though Laskin *et al.* [6] show that contrastive learning outperforms an AE in representation power, the required data augmentation, e.g., cropping or rotating the input image, cannot be transferred to local sensor data.

The four contributions of our work, which mainly address the characteristics of the latent space as well as the incor-

All authors are with the Humanoid Robots Lab, University of Bonn, Germany. This work has partly been supported by the German Research Foundation under Germany's Excellence Strategy, EXC-2070 - 390732324 (PhenoRob).

porated information within, are the following. At first, we propose a, to our best knowledge, novel preprocessing to improve the general reconstruction performance, especially in cluttered regions and around sharp edges. We then train a variational autoencoder (VAE) to compress and reconstruct the preprocessed input into a probability distribution, see Fig. 1 for an example. In comparison to existing approaches [7], [8], [9], we focus on a compact latent space and, additionally, aim for high, but uncorrelated, activity of each latent dimension, also known as disentangled representation [10]. Finally, we are investigating the capability of incorporating time-dependent knowledge into the latent space by using a memory model based on Ha *et al.* [11]. The neural networks are implemented and optimized using tensorflow [12]. The simulated datasets are generated with pybullet [13] and the real-world dataset is recorded with a slamtec rplidar A3. In our experimental evaluation, we show the reconstruction power of our approach, as well as the compactness of the resulting state representation and the capability to incorporate time-dependent information.

II. RELATED WORK

A lot of the related work in the area of autoencoding lidar scans focuses, different from ours, on the reconstruction of 3D data. Gaccia *et al.* [14] reconstruct 3D-lidar data recorded in outdoor environments. The focus lays on the preprocessing into a 2D grid and the reconstruction of corrupted data, e.g., by noise, to recover the original scan. Nicolai *et al.* [15] use the denoising effect to improve estimation of motion in SE(3) for odometry refinement. However, the major purpose of the deep AE is to denoise the 3D-lidar scan, while the scan matching is performed using the reconstructed scan. While we focus on a compact state representation, both works are rather interested in the generative capabilities of the autencoder. Similarly, Yin *et al.* [16] concentrate on autoencoding 3D-lidar data for odometry refinement. The authors investigate the interest point selection by two parallel autoencoding pipelines, using a 2D image and 3D voxel grid representation of the 3D-lidar data. The received interest points are further used for odometry refinement.

Korthals *et al.* [17] apply a VAE for multi modal sensor fusion. The authors encode a 2D-lidar scan and RGB image of the identical scene to fuse them using a third encoder. This work does focus on 2D-lidar data, however, the latent space itself and its compactness is not further discussed. Lundell *et al.* [7] use an AE to reconstruct range measurements that are minimal along the complete height of the robot. This is required, when the obstacle is below or above the height level of the range measurements but the robot itself would hit the obstacle, e.g., in the case of a table. The purpose is to support the navigation using the reconstructed data, while the latent space itself is not further considered.

Schlichting *et al.* [8] train an AE to reduce the dimensionality of a 2D-lidar scan from an outdoor scene. For localization, matching scans are computed with a k-means clustering algorithm directly in the latent space. The work analyzes the size of the latent space, but rather in context

of scan matching performance than actual compactness of the latent space. Wakita *et al.* [9] apply a VAE for map-construction and self-localization. A previously stored combination of features and a global pose is used to find the closest match in feature space with the current encoded scan. The final pose is determined by decoding the stored features and match the current scan using ICP. The authors mention a blurring on sharp edges, also called step edge. This effect appears in the reconstructed input, when a high difference between neighboring range measurements due to the shape of the observed obstacle is present.

We noticed that step edges only occur when directly using the 1D array of the raw range measurements as input. Therefore, we present a novel preprocessing for autoencoding 2D-lidar scans to overcome the problem of step edges. We further investigate the capability of maximal compression with lossless reconstruction, as well as the correlation between each of the latent dimensions. As the required information for navigation tasks is not fully included within a single lidar scan, e.g., ego-motion, we also add this knowledge by applying a memory model first proposed by Ha *et al.* [11].

III. BACKGROUND

In this section we briefly outline the required background including the variational autoencoder (VAE) [18] and the state-of-the-art disentangling methods.

A. Variational Autoencoder

Autoencoders (AE) in general consist of an encoder or recognition model q , which compresses the data x into a latent space $z \in \mathbb{R}^k$. The dimension or compactness of the latent space is given by the hyperparameter k . The second part of an AE is the decoder or generative model p , which returns the reconstructed input x' given the latent space. The target is to minimize the error between x and x' .

While the original concept of an AE is deterministic, Kingma *et al.* [18] applied amortized variational inference to propose a stochastic AE, known as variational autoencoder. The recognition model $q(z|x)$ is changed to return a distribution over the latent space, which captures uncertainty. The generative model $p(x'|z)$ returns a distribution over the reconstructed input given the latent space. Commonly, both models are parametrized by a neural network. The target is formulated by maximizing a variational lower bound on the marginalized log-likelihood of the generative model

$$\log p(x) \geq \mathbb{E}_q [\log p(x|z)] - \beta \cdot D_{\text{KL}}(q(z|x) || p(z)). \quad (1)$$

The scaling factor β will be introduced in the next section and for now is assumed to be 1. Intuitively, the first term on the right in the above equation can be interpreted as a reconstruction loss. The second term is a penalty to prevent that the recognition model is too deterministic and concurrently maintain its simplicity. More precisely, the reconstruction term maximizes the log-likelihood of the generative model under the expectation of the recognition model. This can be directly computed, while the expectation can be estimated

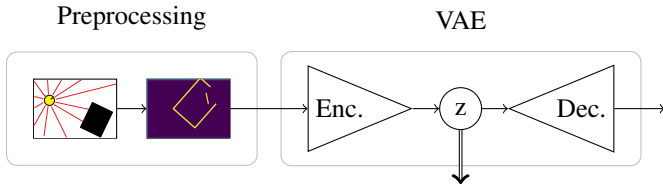


Fig. 2: Proposed autoencoding pipeline. The range measurements are preprocessed into the local image. The encoder compresses the image into a stochastic latent space z . This is the quantity of interest, as marked by the double arrow. The decoder reconstructs a distribution over the original image.

with one sample if the batch size is large enough [18]. The penalty for simplicity is a distance measure, represented by the Kullback-Leibler (KL) divergence, between the recognition model and a prior $p(z)$. The prior is commonly defined by a diagonal standard Gaussian to emphasize the recognition model to be simple. Especially the factorized character of the prior has an important role, as discussed in the next section.

B. Disentanglement

Disentanglement describes the correlation between one key factor of a dataset, e.g., age or skin color in the context of face recognition, and one specific latent dimensions [10]. Each dimension should correlate with exactly one factor, while not being effected by any of the others. VAE naturally induce disentanglement due to the penalty given by the KL divergence. The factorized character of the prior emphasizes the latent space dimensions to be disentangled. Higgins *et al.* [19] amplify this effect by introducing the above mentioned hyperparameter $\beta \geq 1.0$, see Eq. (1).

Kim *et al.* [20] further investigated the composition of the KL divergence. The term splits up into the mutual information between x and z as well as a KL divergence between the factorized prior and the marginalized recognition model $q(z)$. The authors argue, that the benefit of β -VAE is originated in the second KL divergence and the loss in reconstruction performance comes with penalizing the mutual information. Only penalizing $D_{\text{KL}}(q(z)||p(z))$ or enforcing the factorizability of $q(z)$ is not feasible, as the marginalization step is too expensive. However, as it is possible to sample from $q(z)$ without knowing it, using the recognition model, one can train a discriminator network to predict whether a sample is drawn from $q(z)$ or from a truly factorized opponent $\bar{q}(z)$. This is trained in an adversarial fashion and added as additional penalty, where the VAE is emphasized to fool the discriminator, while the latter tries to precisely tell samples from $q(z)$ and $\bar{q}(z)$ apart.

IV. PROPOSED AUTOENCODING PIPELINE

In this section we describe each step of our autoencoding pipeline for 2D-lidar scans. The interest is to train a compact and meaningful state representation for further usage in a RL setup for navigation tasks. An overview is given in Fig. 2. At first we introduce a novel preprocessing for autoencoding 2D-lidar scans and then present the network architecture alongside with the important hyperparameters. Finally, we

Encoder	Decoder
Input: 320 × 320 local image	Input: latent sample $\in \mathbb{R}^k$
Conv. 32 × 3 × 3, stride 2 ReLU, BN	Dense, 256, ReLU
Max pool. 2 × 2	Dense, 5 × 5 × 128, ReLU reshaped
Conv. 32 × 3 × 3, stride 2 ReLU, BN	Trans. Conv., 128 × 3 × 3 stride 2, ReLU
Conv. 64 × 3 × 3, stride 1 ReLU, BN	Trans. Conv., 64 × 3 × 3 stride 2, ReLU
Avg. pool. 2 × 2	Trans. Conv., 64 × 3 × 3 stride 2, ReLU
Conv. 128 × 3 × 3, stride 2 ReLU, BN	Trans. Conv., 32 × 3 × 3 stride 2, ReLU
Conv. 128 × 3 × 3, stride 2 ReLU, BN, flatten	Trans. Conv., 32 × 3 × 3 stride 2, ReLU
Dense, 256, ReLU	Trans. Conv., 32 × 3 × 3 stride 2, ReLU
Dense, 2k	Conv. 1 × 3 × 3, stride 1
Output: Diag. Gaussian	Output: Ind. Bernoulli

TABLE I: Network architecture from top to bottom.

focus on incorporating time-dependent information, as egomotion, into the latent space by applying a memory model.

A. Preprocessing

Wakita *et al.* [9] mention that a VAE smooths sharp edges during reconstruction. We had similar observations and additionally noticed even worse behavior in cluttered areas, where the ranges of neighboring measurements underlay a lot of change. During our work we observed that this behavior is originated in the incapability of the VAE to understand the geometric correlation between the scans in Cartesian space based on raw range measurements.

To overcome this, we preprocess the range measurements r into a local, egocentric map, representing the occupancy in a 20 m × 20 m area around the sensor. First, we normalize the data with a maximum range of 10 m into the interval $\bar{r} \in [0, 1]$ and set every measurement that is invalid or outside this range to zero. The normalized polar coordinates are then converted into Cartesian space and casted to indices after multiplying them with the desired map resolution. The indices are used to compute the desired binary image, referred to as local image. Of particular note is that our local image only requires local sensor data and no global information, in contrast to the one proposed by Regier *et al.* [21].

B. Network Architecture

Our network architecture for the VAE is shown in Tab. I. Each of the convolutional layers that are marked with a *BN* have a preceding batch normalization layer [22]. The final layers of the encoder and decoder are distribution layers [23]. For the encoder we used a diagonal Gaussian distribution and an independent Bernoulli distribution for the decoder. Regarding the encoder, the second dense layer is used to parametrize the diagonal Gaussian distribution and therefore has 2k nodes, per latent dimension the mean value and the standard deviation.

C. Memory Model

A navigation task cannot be solved purely based on a single sensor scan, because time-dependent quantities such as direction of travel and velocity are hidden. While it is possible to pass these information in addition, our proposed state representation already inherits them. As a result, the agent does not need to learn a correlation between the state and ego-motion as it is already represented. Inspired by Lee *et al.* [24], we apply a memory model in combination with the VAE to incorporate such information into the latent representation.

The VAE architecture described in the previous section is not changed. Concurrently with the VAE, a memory model is trained to predict based on a given initial state and a series of actions a future distribution over the latent space $\hat{q}(z|h, a)$, which we refer to as predictive model. The predictive model \hat{q} is optimized to be similar to the recognition model q . Additionally, the target is to minimize the error between the actual future scan and the reconstruction based on a sample from the predictive model. We slightly modified the loss function in Eq. (1) to meet the above requirements

$$\begin{aligned} L = & \sum_{t=0}^T \mathbb{E}_{q(z|x)} [\log p(x_t|z_t)] - D_{KL}(q(z_t|x_t)||p(z)) \\ & + \sum_{t=1}^T \mathbb{E}_{\hat{q}(z_t|h_t, a_{t-1})} [\log p(x_t|z_t)] \\ & - \sum_{t=1}^T D_{KL}(\hat{q}(z_t|h_t, a_{t-1})||q(z_t|x_t)). \end{aligned} \quad (2)$$

The first two terms are identical to the VAE setup but sum over the entire sequence. The second line is the reconstruction term for the predictive model \hat{q} . We are not summing over the entire sequence as the prediction starts with the second scan. The last term encourages the predictive model to have a similar distribution as the recognition model for the same time step by penalizing the KL divergence. In the first time step the predictive model is initialized with a sample from the recognition model. However, afterwards it only receives its previous states and the executed action, i.e., rotational and translational velocity commands.

While Lee *et al.* [24] use two stochastic layer, for our memory model a GRU [25] network with one layer and 256 units works best. As we require a distribution over the predicted latent space and a GRU network is deterministic, we use a subsequent stochastic layer. The latter is represented by two dense layers and parametrizes based on the GRU's hidden state a diagonal Gaussian distribution, which has the same shape as the one from the recognition model.

Concluding, we have introduced a novel preprocessing as well as our network structure to encode lidar scans into a compact and meaningful state representation. To incorporate time-dependent knowledge, we proposed a memory model.

V. EXPERIMENTAL EVALUATION

In this section we present experiments to evaluate our autoencoding pipeline for 2D-lidar data. In particular, we

first demonstrate the increased reconstruction power due to the preprocessing into our local image. Afterwards we show the impact of current state-of-the-art disentangling methods on the latent space regarding the general activity of each dimensions. Finally, we show the ability of the memory model to include time-dependent information.

A. Experimental Environments

First, we shortly introduce the characteristics of our experimental environments. We simulated two different categories of environments using pybullet [13]. The simulations are at a rate of 5 Hz and to mimic noisy sensors we randomly invalidated measurements. The first category consists of a small rectangular room. Both side lengths are uniformly drawn from $l \in [4 \text{ m}, 8 \text{ m}]$ and a small round pole with a diameter of 0.2 m is placed at random in the room. During simulation the robot is set to different poses and randomly drives through the environment until a collision occurs or a maximum number of steps is reached. We collected 10 trajectories per room with 250 randomly sampled rooms in total. This dataset is referred to as *simple environment*, see Fig. 3 as an example.

In a next step, we slightly increased the room size to $l \in [5 \text{ m}, 10 \text{ m}]$ and added additional walls as well as increased the number of poles, which now can be round and square with alternating diameter $d \in [0.1 \text{ m}, 0.4 \text{ m}]$. The likelihood of poles being placed close to each other or in corners is increased to simulate cluttered regions. We simulated 250 trajectories per room, at a total number of 100 rooms. This dataset is referred to as *complex environment*, see Fig. 5 as an example. For the memory model we additionally require smoother action-trajectories, as these are part of the dataset to understand the robots kinematics. We generated these by applying different action selection schemes: Random, wide left/right curve, serpentine motion forward, static left/right rotation, and straight motion forward. To ensure a steady but random motion the actions are drawn uniformly but with a minimal value. The sign of the actions are fix and given by the selective schemes described above.

For the real-world experiments we collected scans with a slamtec rplidar A3 attached to a turtlebot. We roughly collected one hour of scans at 20 Hz within our entire building, including hallways, offices, kitchens, and labs. This dataset is referred to as *real environment*, see Fig. 1 as an example. We use for the real and simple environment a latent dimension of $k = 16$ and for the complex environment a dimension of $k = 32$. Both values turned out to be the minimal value without noticing a greater reconstruction loss.

B. Reconstruction Error

In this section, we are showing the improvement due to our preprocessing. We used a resolution of 320 pixel for the local image, which corresponds to 6.25 cm per pixel in a $20 \text{ m} \times 20 \text{ m}$ area. This resolution provides enough information for cluttered regions, without being to expensive in computation. Regarding the experiments, when trained directly on the raw range measurements, the network architecture of the

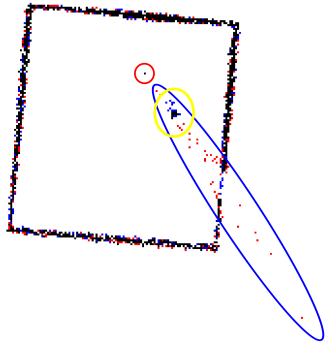


Fig. 3: Reconstruction sample from the simple environment. We compare the autoencoding pipeline based on our local image and on raw measurements. False positives are marked in color, blue ones are based on the local image and red ones on raw measurements. The robot pose is highlighted with a red circle, which is not in the center as we cropped the free space. The pole is highlighted with a yellow circle. As can be seen the undesired blurred edge occurs only with the raw measurements (as highlighted with a blue circle).

recognition model is strongly related to the one used by Pfeiffer *et al.* [26], which we refer to for further details. For the convolutional layer, we used circular padding [27]. The generative model is similar to the one proposed in Tab. I, but we adapted the filter numbers, kernel sizes and strides to meet the encoder and data structure. Additionally, we had to take the average of neighboring measurements if the actual measurement was invalid, as setting it to zero heavily decreased the performance.

In Fig. 3 we compare the two methods on a sample from the simple environment. As can be seen learning on raw measurements blurs sharp edges, which increases false positives (colored pixel). The blurred edge is highlighted by the blue circle, caused by the pole (yellow circle) and the suddenly changing range measurements. This behavior does not occur when we use our local image as input.

To further compare both methods we averaged the false positives and false negatives over each of the datasets. As many errors appear close to walls, see Fig. 3, and are less critical, we additionally use a corrected version of each measure. The scores are described and listed in Tab. II. The table shows, that the local image increases the performance in each environment. Only the false negatives in the simple environment are slightly worse, but in a neglectable magnitude. Furthermore, even for unseen rooms or in a different environment category the autoencoder captures the relevant parts, such as walls and greater cluttered regions, and is almost capable of keeping the level of performance. When transferring the autoencoder for the simple environment from simulation into a similar real-world environment without retraining, especially the false positives increase, which also impacts on the MSE. This is actually expected, as the average number of occupied pixels dropped by a factor of roughly 2.6 from simulation to real world, and therefore the autoencoder expected more pixels to be occupied for the same shapes. However, all walls and the pole are correctly reconstructed, as can be seen in the accompanying video. As we further noticed a slight drop in performance for the real dataset in

Train	Eval.		FP	cFP	FN	cFN	MSE
Simple	Simple	our	0.325	0.018	0.328	0.012	0.326
		raw	0.362	0.043	0.323	0.015	0.643
Simple	Real	our	1.231	0.219	0.173	0.013	0.859
		raw	0.340	0.033	0.343	0.022	0.347
Comp.	Simple	our	0.386	0.063	0.406	0.042	0.398
		raw	0.487	0.139	0.407	0.055	0.827
Comp.	unseen	our	0.432	0.091	0.428	0.063	0.446
		raw	1.684	1.264	0.594	0.312	1.440
Real	Real	our	0.429	0.144	0.432	0.106	0.444
		raw	1.529	1.130	0.548	0.277	1.361
Real, 20 Hz	Real, 20 Hz	our	0.492	0.201	0.523	0.158	0.512
		raw	1.529	1.130	0.548	0.277	1.361

TABLE II: Normalized error for the preprocessing methods within each of the complete datasets. The local image is indicated by *our*, the raw measurements by *raw*. The first column indicates in which environment the autoencoder is trained, the second in which it is evaluated. We average false positives (FP) and false negatives (FN) per image over each dataset. The corrected false positives (cFP) are computed by removing the FP, that are next to a truly occupied pixel. False negative pixels next to a positively estimated pixel are removed to get the corrected false negatives (cFN). These quantities are computed based on samples from the generative model. To also take the mean probability into account we computed the mean squared error (MSE) for the expectation of the generative model. Each score is normalized by the average number of occupied pixels per image in a dataset. Our pipeline based on the local image clearly outperforms the one based on raw range measurements. After Welch's t-test [28] the local image leads to a significantly smaller MSE on all datasets (for a level of 0.01). The second and fifth row show the performance of the autoencoder trained on the complex dataset, but tested in the simple environment and on unseen rooms. The third row represents the transfer from the simple environment into a similarly rebuild real world environment, as also can be seen in the accompanying video.

comparison to our simulation, we downsampled the dataset from 20 Hz to 5 Hz to remove almost identical scans. This increases the difficulty of the learning task and therefore forces the network to further generalize. The table shows that this actually improves the reconstruction results. Note that for the VAE based on raw measurements the downsampling made the scores worse as it overfits.

C. Disentanglement

In this section we investigate the activity of each latent dimension when applying current state-of-the-art disentangling methods on prerecorded sequences within the simple environment. These sequences contain 100 consecutive scans with simple motion patterns, e.g., driving forward facing a wall and stopping right in front of it. However, it is impossible to directly quantify the degree of disentanglement, as the key factors (see Sec. III) of our datasets are unknown and difficult to define at all. We still assume that each of the sequences only interferes with a limited set of key factors and therefore should have a minimal number of active latent dimensions or, in general, low activity.

This is evaluated in Fig. 4 with one network per β -value. For β -VAE [19] increasing β to emphasize disentanglement clearly reduces the general activity, while especially the least active dimensions keep getting less active. In contrast the most active dimensions stay, except the outlier, at the

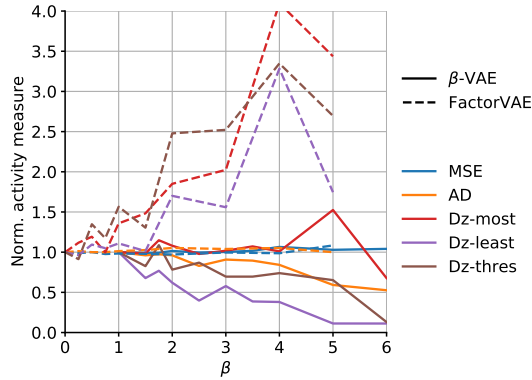


Fig. 4: Quantification of latent space activity under different degrees of disentanglement, represented by β . The values for β -VAE start at $\beta = 1$, which is a basic VAE. For FactorVAE the penalty comes in addition to the VAE cost function and therefore starts at $\beta = 0$. We computed the mean squared error (MSE) from Tab. II and counted the number of active dimensions (AD). We used the difference in z (Dz) for consecutive scans and compute the average over the most active (Dz-most) and least active dimensions (Dz-least). At last we counted the dimensions whose difference at least once exceeded a threshold (Dz-thres). All values are normalized by the values of a basic VAE. As can be seen, all values from β -VAE drop with increasing beta, besides the ones that are important for carrying the information (Dz-most), as concurrently the MSE stays almost constant. FactorVAE does not lead to this behavior.

same level of activity, which is desirable as these carry the relevant information. Concurrently, the reconstruction error only slightly increases. Generally, the bigger β the better, but above $\beta = 2.5$ fine structures as the pole start to disappear due to generalization. FactorVAE [20] required a lot of additional fine tuning and unfortunately did not result in the desired activity reduction.

D. Motion Prediction

In this section we evaluate the performance of the memory model. The purpose is to incorporate all time-dependent knowledge within the latent space to be able to fully rely on this state representation without additional sources of information. This makes the later need to understand the relation between motion and the state unnecessary. The purpose of the memory model is to capture time-dependent information along one sequence, which in our experiments consists of ten consecutive scans at a rate of 5 Hz. Fig. 5 shows for a given sequence the first and last scan, as well as a decoded sample from the recognition and predictive model for the last scan. It is obvious that the rotational and translational change is captured almost perfectly by the memory model (bottom right), while only the sharpness of the short wall in the free space is lost.

To further show the capability of including time-dependent information within the state representation, we trained a one-layered network to predict the current velocity. The recognition and memory model are part of the preprocessing for this experiment and the resulting latent space acts as input. When the memory model is not incorporated, the velocity predictions are basically random. Unfortunately, with the memory model the error barely drops. In comparison, when

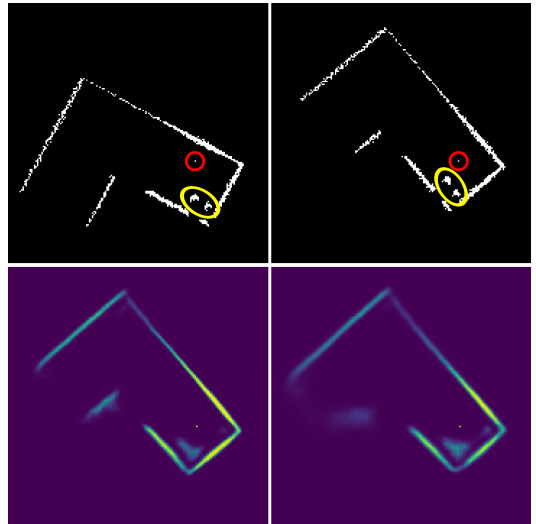


Fig. 5: Future prediction of the memory model. Top left shows the initial state, on the top right is the future state that needs to be predicted. The robot pose is highlighted with a red circle and poles with a yellow circle. The image on the bottom left shows the reconstruction from the recognition model. The reconstruction from the predictive model purely based on the initial state and the sequence of actions is on the bottom right. All four images are cropped identically to reduce visible free space. It can be seen that the memory model almost perfectly predicts the future scan.

directly trained on the hidden state of the memory model, the network error is heavily reduced and leads to an almost perfect velocity prediction. We argue that the recognition model forgets the hidden state as it is not required for the scan reconstruction. We counter that, by adding a penalty for reconstructing the hidden state of the memory model based on the latent space. This ensures, that the information stays within the latent space, without using any target quantity, e.g., the velocity itself. Using a small weighting factor for the penalty does not change the performance when reconstructing the lidar scan, but reduces the velocity prediction by one magnitude. This is almost as good as directly predicting based on the hidden state, and already perfectly captures the major direction of travel with minor offset. This shows, that our autoencoding pipeline is capable of incorporating further knowledge into the latent space, as long as this information is task-relevant and captured by the objective.

VI. CONCLUSION

In this paper, we presented an autoencoding pipeline for 2D-lidar data and proposed a novel preprocessing that improved the overall performance in comparison to autoencoding the raw sensor data. We evaluated the compactness and correlation of our state representation using simulated and real-world data. To show that further knowledge can be incorporated within the state representation, we trained concurrently a memory model to capture the ego-motion of the sensor. Based on our state representation, already a small network can predict time-dependent information. Concluding, our autoencoding pipeline is capable of incorporating highly relevant information for a navigation task within a compact state representation.

REFERENCES

- [1] G. Ferrer, A. G. Zulueta, F. Cotarelo, and A. Sanfeliu, “Robot social-aware navigation framework to accompany people walking side-by-side,” *Autonomous Robots*, 2017.
- [2] C. Chen, Y. Liu, S. Kreiss, and A. Alahi, “Crowd-Robot Interaction: Crowd-Aware Robot Navigation With Attention-Based Deep Reinforcement Learning,” *Proc. of the IEEE Intl. Conf. on Robotics & Automation (ICRA)*, 2018.
- [3] D. Yarats, A. Zhang, I. Kostrikov, B. Amos, J. Pineau, and R. Fergus, “Improving sample efficiency in model-free reinforcement learning from images,” *arXiv preprint*, 2019.
- [4] C. Finn, X. Y. Tan, Y. Duan, T. Darrell, S. Levine, and P. Abbeel, “Deep spatial autoencoders for visuomotor learning,” *Proc. of the IEEE Intl. Conf. on Robotics & Automation (ICRA)*, 2016.
- [5] M. Jaderberg, V. Mnih, W. M. Czarnecki, T. Schaul, J. Z. Leibo, D. Silver, and K. Kavukcuoglu, “Reinforcement Learning with Unsupervised Auxiliary Tasks,” *CoRR*, 2016.
- [6] M. Laskin, A. Srinivas, and P. Abbeel, “Curl: Contrastive unsupervised representations for reinforcement learning,” *Proc. of the Intl. Conf. on Machine Learning (ICML)*, 2020.
- [7] J. Lundell, F. Verdoja, and V. Kyrki, “Hallucinating robots: Inferring obstacle distances from partial laser measurements,” *Proc. of the IEEE/RSJ Intl. Conf. on Intelligent Robots and Systems (IROS)*, 2018.
- [8] A. Schlichting and U. Feuerhake, “Global vehicle localization by sequence analysis using lidar features derived by an autoencoder,” in *IEEE Intelligent Vehicles Symposium*, 2018.
- [9] S. Wakita, T. Nakamura, and H. Hachiya, “Laser variational autoencoder for map construction and self-localization,” in *Proc. of the IEEE Intl. Conf. on Systems, Man, and Cybernetics (SMC)*, 2018.
- [10] Y. Bengio, A. Courville, and P. Vincent, “Representation learning: A review and new perspectives,” *IEEE Trans. on Pattern Analysis and Machine Intelligence (TPAMI)*, 2013.
- [11] D. Ha and J. Schmidhuber, “World models,” *CoRR*, 2018.
- [12] M. Abadi, A. Agarwal, P. Barham, E. Brevdo, Z. Chen, C. Citro, G. S. Corrado, A. Davis, J. Dean, M. Devin, S. Ghemawat, I. Goodfellow, A. Harp, G. Irving, M. Isard, Y. Jia, R. Jozefowicz, L. Kaiser, M. Kudlur, J. Levenberg, D. Mané, R. Monga, S. Moore, D. Murray, C. Olah, M. Schuster, J. Shlens, B. Steiner, I. Sutskever, K. Talwar, P. Tucker, V. Vanhoucke, V. Vasudevan, F. Viégas, O. Vinyals, P. Warden, M. Wattenberg, M. Wicke, Y. Yu, and X. Zheng, “TensorFlow: Large-scale machine learning on heterogeneous systems,” 2015, software available from tensorflow.org. [Online]. Available: <https://www.tensorflow.org/>
- [13] E. Coumans and Y. Bai, “PyBullet, a Python module for physics simulation for games, robotics and machine learning,” <http://pybullet.org>, 2016–2019.
- [14] L. Caccia, H. v. Hoof, A. Courville, and J. Pineau, “Deep generative modeling of lidar data,” *Proc. of the IEEE/RSJ Intl. Conf. on Intelligent Robots and Systems (IROS)*, 2019.
- [15] A. Nicolai and G. A. Hollinger, “Denoising autoencoders for laser-based scan registration,” *IEEE Robotics and Automation Letters*, 2018.
- [16] D. Yin, Q. Zhang, J. Liu, X. Liang, Y. Wang, J. Maanpää, H. Ma, J. Hyppä, and R. Chen, “Cae-lo: Lidar odometry leveraging fully unsupervised convolutional auto-encoder for interest point detection and feature description,” *arXiv preprint*, 2020.
- [17] T. Korthals, M. Hesse, J. Leitner, A. Melnik, and U. Rückert, “Jointly trained variational autoencoder for multi-modal sensor fusion,” *Proc. of the Int. Conf. on Information Fusion (FUSION)*, 2019.
- [18] D. P. Kingma and M. Welling, “Auto-encoding variational bayes,” *Intl. Conf. on Learning Representations (ICLR)*, 2013.
- [19] I. Higgins, L. Matthey, A. Pal, C. Burgess, X. Glorot, M. Botvinick, S. Mohamed, and A. Lerchner, “beta-vae: Learning basic visual concepts with a constrained variational framework,” in *Intl. Conf. on Learning Representations (ICLR)*, 2017.
- [20] H. Kim and A. Mnih, “Disentangling by factorising,” 2018.
- [21] P. Regier, L. Gesing, and M. Bennewitz, “Deep reinforcement learning for navigation in cluttered environments,” *Proc. of the Intl. Conf. on Machine Learning and Applications (CMLA)*, 2020.
- [22] S. Ioffe and C. Szegedy, “Batch Normalization: Accelerating Deep Network Training by Reducing Internal Covariate Shift,” in *Proc. of the Intl. Conf. on Machine Learning (ICML)*, 2015.
- [23] J. V. Dillon, I. Langmore, D. Tran, E. Brevdo, S. Vasudevan, D. Moore, B. Patton, A. Alemi, M. D. Hoffman, and R. A. Saurous, “Tensorflow distributions,” *CoRR*, 2017.
- [24] A. X. Lee, A. Nagabandi, P. Abbeel, and S. Levine, “Stochastic latent actor-critic: Deep reinforcement learning with a latent variable model,” *arXiv preprint*, 2019.
- [25] K. Cho, B. van Merriënboer, Ç. Gülcühre, F. Bougares, H. Schwenk, and Y. Bengio, “Learning phrase representations using RNN encoder-decoder for statistical machine translation,” *CoRR*, 2014.
- [26] M. Pfeiffer, M. Schaeuble, J. I. Nieto, R. Siegwart, and C. Cadena, “From Perception to Decision: A Data-driven Approach to End-to-end Motion Planning for Autonomous Ground Robots,” *CoRR*, 2016.
- [27] S. Schubert, P. Neubert, J. Pöschmann, and P. Pretzel, “Circular Convolutional Neural Networks for Panoramic Images and Laser Data,” in *Proc. of the IEEE Intelligent Vehicles Symposium (IV)*, 2019.
- [28] B. L. Welch, “The generalization of ‘student’s’ problem when several different population variances are involved,” *Biometrika*, 1947.